PAPER • OPEN ACCESS

RFX-mod2 as a flexible device for reversed-field-pinch and low-field tokamak research

To cite this article: D. Terranova *et al* 2024 *Nucl. Fusion* **64** 076003

OPEN ACCESS
IOP Publishing | International Atomic Energy Agency
Nuclear Fusion
Nucl. Fusion **64** (2024) 076003 (13pp)
https://doi.org/10.1088/1741-4326/ad4805

RFX-mod2 as a flexible device for reversed-field-pinch and low-field tokamak research

D. Terranova[1,2,*], M. Agostini[1,2], F. Auriemma[1,2], M. Gobbin[1,2], G. Marchiori[1,2], L. Pigatto[1], P. Porcu[1,4], I. Predebon[1,2], G. Spizzo[1,2], N. Vianello[1,2], P. Zanca[1], D. Abate[1], T. Bolzonella[1], D. Bonfiglio[1,2], M. Bonotto[1], S. Cappello[1,2], L. Carraro[1,2], R. Cavazzana[1], P. Franz[1], R. Lorenzini[1,3], L. Marrelli[1,2], R. Milazzo[2], S. Peruzzo[2], M.E. Puiatti[1], P. Scarin[1], M. Spolaore[1,2], E. Tomasina[1,4], M. Valisa[1,2], M. Veranda[1,2], B. Zaniol[1] and M. Zuin[1,2]

[1] Consorzio RFX (CNR, ENEA, INFN, Università di Padova, Acciaierie Venete SpA), Padova, Italy
[2] Istituto per la Scienza e la Tecnologia dei Plasmi (ISTP), CNR, Padova, Italy
[3] ENEA - Centro Ricerche Bologna, Bologna, Italy
[4] Centro Ricerche Fusione—Università di Padova, Padova, Italy

E-mail: david.terranova@igi.cnr.it

Received 15 January 2024, revised 5 April 2024
Accepted for publication 7 May 2024
Published 20 May 2024

Abstract
The RFX-mod2 installation is planned to be completed by 2024 and the start of operations is expected in 2025. The high flexibility of the machine (already tested in the previous RFX-mod experiment) allows operation in Reversed Field Pinch and tokamak configuration as well as ultra-low q pulses. In this work we present predictive analysis on transport, performances and plasma control in RFX-mod2 in view of the first experimental campaigns.

Keywords: RFP, tokamak, transport, MHD, plasma control

(Some figures may appear in colour only in the online journal)

1. Introduction

RFX-mod2 [1] originates from the modification of the former RFX-mod machine design in order to reduce the plasma-shell distance (b/a from 0.51 m/0.459 m = 1.11 for RFX-mod to 0.51 m/0.49 m = 1.04 for RFX-mod2, where b and a are the shell and first wall minor radius, respectively) and remove the highly resistive Inconel vessel, deemed responsible of a very low wall-locking threshold for tearing modes (TMs) [1]. RFX-mod operated between 2004 and 2015, being itself a modified version of the original Reversed Field eXperiment (RFX, 1992–1999). The new RFX-mod2 experiment is presently being assembled [2] and is expected to start operation in 2025. Like RFX-mod, thanks to the high flexibility of its power supplies the machine will operate both in tokamak and Reversed Field Pinch (RFP) configuration as well as producing ultra-low q plasmas [3, 4]. In this respect, the machine will also benefit from a largely improved and extended set of diagnostics [5] that will allow a better analysis of experiments in all magnetic configurations, with a significant improvement for tokamak plasmas.

Given the design of the new copper shell, we expect that error fields due to passive structures and the amplitude of MHD modes in the RFP configuration will be reduced [1]. This will open new operational scenarios (e.g. spontaneous mode rotation at higher plasma current and further reduction of plasma wall interaction) with improved plasma performance.

* Author to whom any correspondence should be addressed.

As for tokamak plasmas, dedicated campaigns will focus on shaped plasmas both in positive (already started in RFX-mod) and negative (completely new operation) triangularity.

In view of the restart of the operations new tools for plasma control (TMs and RWM modes) are in preparation exploiting the upgraded system of magnetic sensors. At the same time predictive studies are being carried out in order to investigate the achievable plasma scenarios in terms of magnetic field fluctuations amplitude, equilibrium configuration, particle and temperature profiles with related transport.

A standardization of some key numerical tools is ongoing including the equilibrium representation (EQDSK files are available both for tokamak and RFP equilibria) that is the basis for all analyses on experimental data (a description of the equilibrium reconstruction procedure can be found in [6] and [7]). The installation of the IMAS infrastructure for data access to RFX-mod2 pulse file is also being considered. These activities are aimed at easing the participation of a broader community of researchers to the RFX-mod2 experimental programme.

The scientific programme of the renewed facility when operated as a RFP includes the advancement of experiments, preliminarily done on RFX-mod, involving stimulated helical regimes [8] (3D equilibria with a helical core associated to the dominant mode in the magnetic fluctuations spectrum) based on the application of magnetic perturbations (MPs) to select the helical pitch (mode feedback control with non-zero reference) of the resulting QSH (Quasi Single Helicity 3D equilibrium) states. Indeed, a favourable action of MP is expected on the basis of 3D nonlinear MHD simulations, indicating a reduction of secondary mode amplitudes, and an increase of the ratio dominant/secondary modes, consistently with a favourable plasma–wall proximity [9, 10]. In particular, simulations show a more efficient magnetic chaos healing effect occurring in QSH regimes based on non-resonant MPs [11].

RFX-mod2 [12] is now in its final assembling phase, and in this paper we present some scenario studies to be used for reference of the first experimental campaign of the new machine. In section 2 we show studies of transport properties with a focus on RFP plasmas, followed in section 3 by the analysis of stability and control tools for both RFP and tokamak configurations. Section 4 is dedicated to shaped tokamak studies and some final remarks are given in section 5.

2. Transport analysis

It is expected that RFX-mod2 in the RFP configuration will show helical equilibria associated to internal transport barriers and a dominant mode in the spectrum of low (m,n) magnetic fluctuations (see figure 8(a) for an example of the resulting flux surfaces). These states, produced in RFX-mod for the first time (with the (1,7) as dominant mode corresponding to the innermost resonant TM), were then observed in all RFP experiments [7, 13, 14]. In RFX-mod2, due to the modified plasma-shell proximity, we expect a favourable trend compared to RFX-mod in terms of transport properties as shown in [15] (the results are presented in figure 1(a) showing the diffusion coefficient as a function of the ratio between the amplitude of secondary and dominant modes as measured at the edge) and reconnection events effects [16, 17] as numerical MHD analyses show a lower level of MPs (figure 1(b)) reducing the plasma shell distance with possibly an increase in the ratio between dominant and secondary modes. This is quite a promising result, given the fact that residual stochasticity in helical states still plays a crucial role in the barrier formation [18].

In terms of transport mechanisms in RFX-mod two candidates were considered as mainly responsible for the energy transport at the internal barrier: secondary TMs and micro-TMs [18, 19]. To study and model these mechanisms, RFX-mod2 synthetic helical equilibria were produced based on RFX-mod pulses but using the actual geometry of the new machine (i.e. larger minor radius from 0.459 m to 0.491 m). Based on these equilibria the ASTRA [20] and ORBIT [21] codes are used to study transport.

The ASTRA code is run in predictive mode, providing the diffusivities, given the expected fluctuation reduction (see figure 1) and computing the resulting kinetic profiles. Different values of transport coefficients are tested to consider the confidence interval on the extrapolation to regimes not obtained in RFX-mod.

The ORBIT code is used to estimate the expected particle diffusion for the new experiment and to obtain an indirect estimate of the energy transport in the assumption of a dominant chaotic mechanism. To this end, the expected level of magnetic field fluctuations is used as input information for the code as described below.

In the ASTRA modelling a 1.5D transport analysis is done considering the actual metrics of the equilibrium (helical flux surfaces). As in [15] the basic assumptions in the core are a diffusion coefficient associated to magnetic fluctuations [22] and a pinch velocity (outward) combining the contributions from the $E \times B$ drift and the ambipolar electric field (linked to T_i and its gradient). As for the RFX-mod edge region, transport was found to be dominated by electrostatic phenomena and we retain this assumption also in RFX-mod2. In figure 2(a) we plot the density profile obtained from the analysis of a synthetic RFX-mod2 pulse and the profiles obtained scaling the stochastic part of the particle diffusion coefficients by a factor 0.75 and 0.5, shown in panel (c) (this corresponds to a scaling with the amplitude of magnetic fluctuations) and scaling by the same factor also the energy diffusion coefficient. The so called 'experimental diffusivities' shown in figure 2(c) are the RFX-mod diffusivities mapped on the RFX-mod2 geometry. The assumption of reducing the magnetic diffusion coefficients on the whole radius and not only in the proximity of the transport barrier reflects the expected global healing of magnetic chaos responsible for core transport due to a generalized reduction of the amplitude of the magnetic spectrum (i.e. reduction of both dominant and secondary modes). It is interesting to note the peaking of the density profiles in the case corresponding to the higher reduction factor (green line in figure 2(a)). Density profiles still retain the usual peak at the edge that comes from the combined effect of pinch velocity and transport processes at the edge. The temperature profiles (figure 2(b)) show a similar

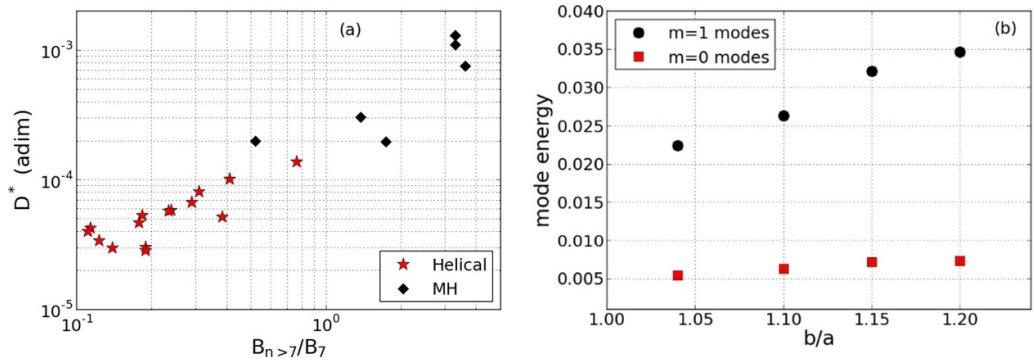

Figure 1. (*a*) Specific diffusivity ($D^* = D/v_{\mathrm{i,th}}$) as a function of relative magnetic fluctuations amplitude (ratio of the amplitude of secondary modes over dominant mode). (*b*) Average normalized mode energy as a function of shell proximity (MHD simulations).

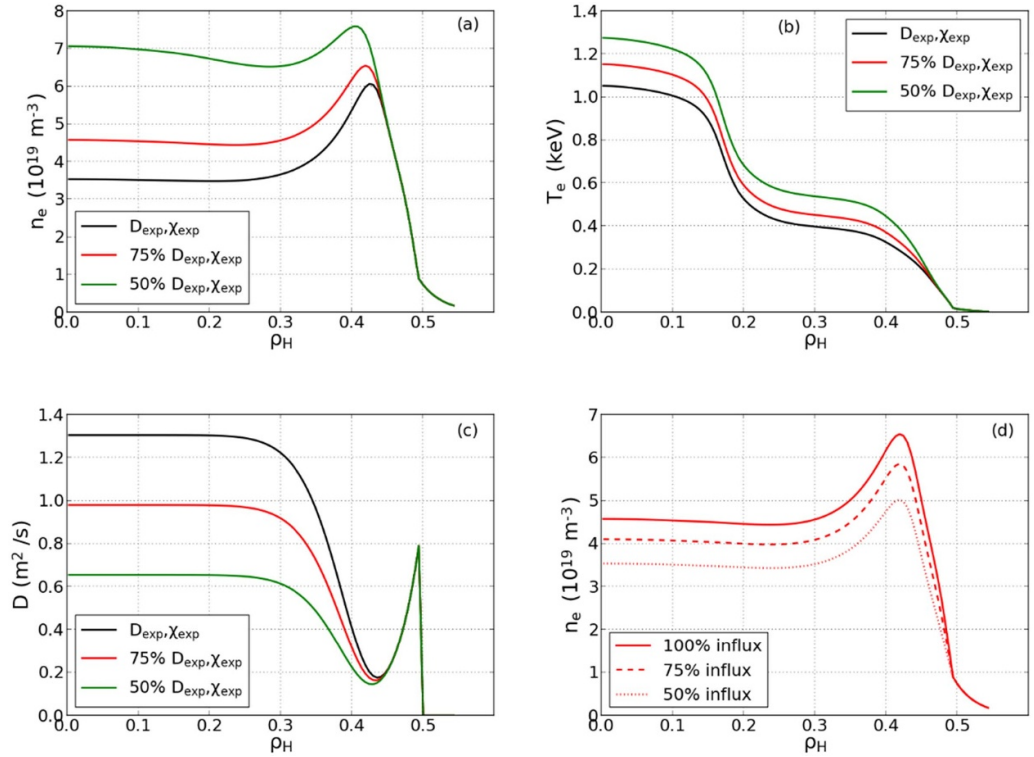

Figure 2. MHD perturbation scaling and ASTRA results: (*a*) plasma density, (*b*) temperature profiles, (*c*) particle diffusion coefficient, (*d*) influxes scaling simulations using as reference diffusion coefficients scaled by 75% (see red profiles). ρ_{H} is the radial flux coordinate of the corresponding equilibrium as in [15].

trend: the reduced transport cases are associated to higher temperatures. This is obtained despite the higher density level and the fact that the input power is kept constant in the simulations. Indeed the reduced transport by a factor 0.75 results in a 36% increase in the total stored energy, while the case with the halved diffusivities shows a 118% stored energy increase.

Since for RFX-mod2 we expect lower error fields and MHD mode amplitudes and therefore a reduced plasma–wall interaction (PWI), we also tested the effect of a reduced level of influxes with ASTRA. For this analysis the starting configuration corresponds to the one with diffusion coefficients scaled by a factor 0.75. As shown in figure 2(*d*) given the reduced amplitude of the particle source the main effect is a down scaling of profiles keeping an almost unchanged shape: the lower density associated to reduced influxes enables a slightly deeper penetration of the particle source which only marginally moves the peak of the density inward. The minimal sensitivity of the shape of the density profile to the particle source penetration is a clear indication that the shape of the density profile is largely driven by transport processes. This is somehow expected since this behaviour was observed also in RFX-mod, i.e. kinetic profiles are defined essentially by transport processes. It is to note that this is a sort of test case analysis as in principle lower influxes may lead to lower edge density which can change the picture of transport at the edge (e.g. larger edge structures could develop): this will be part of actual experiments. To explore such dependencies, we have already

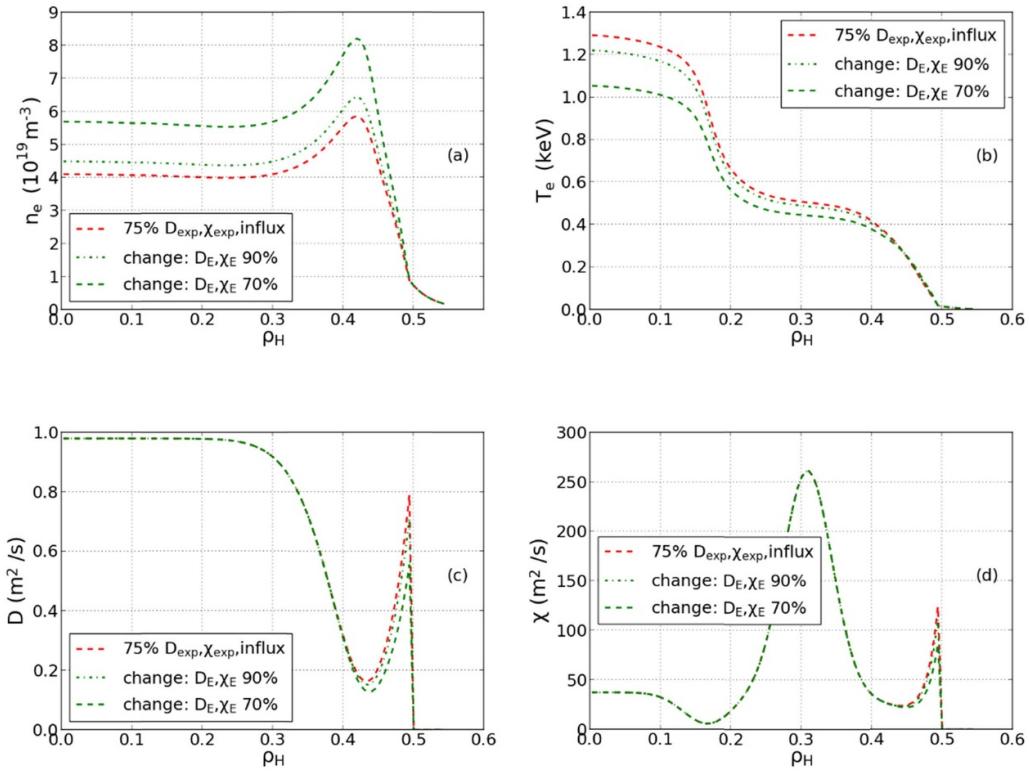

Figure 3. ASTRA analysis scaling electrostatic transport coefficients ($D_{\rm E}$ and $\chi_{\rm E}$) taking as reference the RFX-mod2 case with D and χ scaled by 75% (see figure 2). (*a*) Plasma density, (*b*) temperature profiles, (*c*) particle diffusion coefficient, (*d*) energy diffusion coefficient. $\rho_{\rm H}$ is the radial flux coordinate of the corresponding equilibrium as in [15].

tested the sensitivity of the scenario scanning the edge transport level.

Indeed, the improved magnetic boundary foreseen on RFX-mod2 might have an impact as well on edge electrostatic transport: despite the high level of magnetic fluctuations, a relevant fraction of particle and energy transport in a RFP can still be ascribed to general convective filamentary transport [23–26]. The reduced MP at the edge is likely to cause a corresponding reduction of the plasma wall interaction and thus less dense boundary plasmas. This would imply a reduction of the edge collisionality which will likely induce a reduction of edge turbulence: this is similar to what is observed in tokamaks and reported in [27]. Furthermore, the reduced PWI might have an impact as well on the edge neutral population and ultimately on the edge perpendicular flow with a possible increase of the $E \times B$ shear with a corresponding further increase of the $\omega_{E\times B}$ damping effect on edge turbulence. Thus, despite the general lack of proper modelling of electrostatic turbulence in the edge of the RFP, a reduction of the convective filamentary contribution to edge particle and energy transport might be envisaged in RFX-mod2.

Given these assumptions, we analysed some ASTRA runs scaling down the electrostatic diffusion coefficient (i.e. reducing diffusion only in the edge region where this mechanism is acting) both for particle ($D_{\rm E}$) and heat ($\chi_{\rm E}$): we take as reference the simulation with the magnetic diffusivity scaled down by a factor 0.75 and with a particle influx reduced at 75% (see dashed line in figure 2(*d*)). The reduced edge transport coefficients are shown in figure 3 (panels (*c*) and (*d*)) where the 90% and 70% reduction are applied. The effect on the whole diffusivity profiles can appear small but, since, in particular, the particle source is located at $\rho_{\rm t} = [0.9–1.0]$, such small modification provides a large effect on the density profile, with density increasing as $D_{\rm e}$ decreases. In these cases $T_{\rm e}$ decreases while density increases (see figure 3 panels (*a*) and (*b*)) because of the constant input power assumption. Only the edge gradient increases as $\chi_{\rm E}$ decreases, but such enhancement does not propagate towards the core. The total stored energy increases respectively by 6% and 22% with respect to the reference case.

In the ASTRA simulations magnetic chaos enters indirectly through a stochastic diffusion coefficient but local magnetic field topology is not taken into account. The diffusion coefficient can be directly computed from magnetic fluctuations [22]. As already stated, we actually used the parametric dependence found in [15], which gives not only the trend, but also the absolute expected absolute value. This is not the case for the ORBIT code [21] (a Hamiltonian guiding centre code) where in order to study particle transport the full 3D topology of the magnetic field is required and considered: to this end along with the equilibrium magnetic field, also profiles of the eigenfunctions of magnetic fluctuations were modelled for RFX-mod2 by scaling the RFX-mod profiles to the expected amplitude for the new machine. An example of Poincaré toroidal map obtained by ORBIT is shown in figures 4(*a*) and (*b*) with the full plasma domain and a zoom in the edge zone

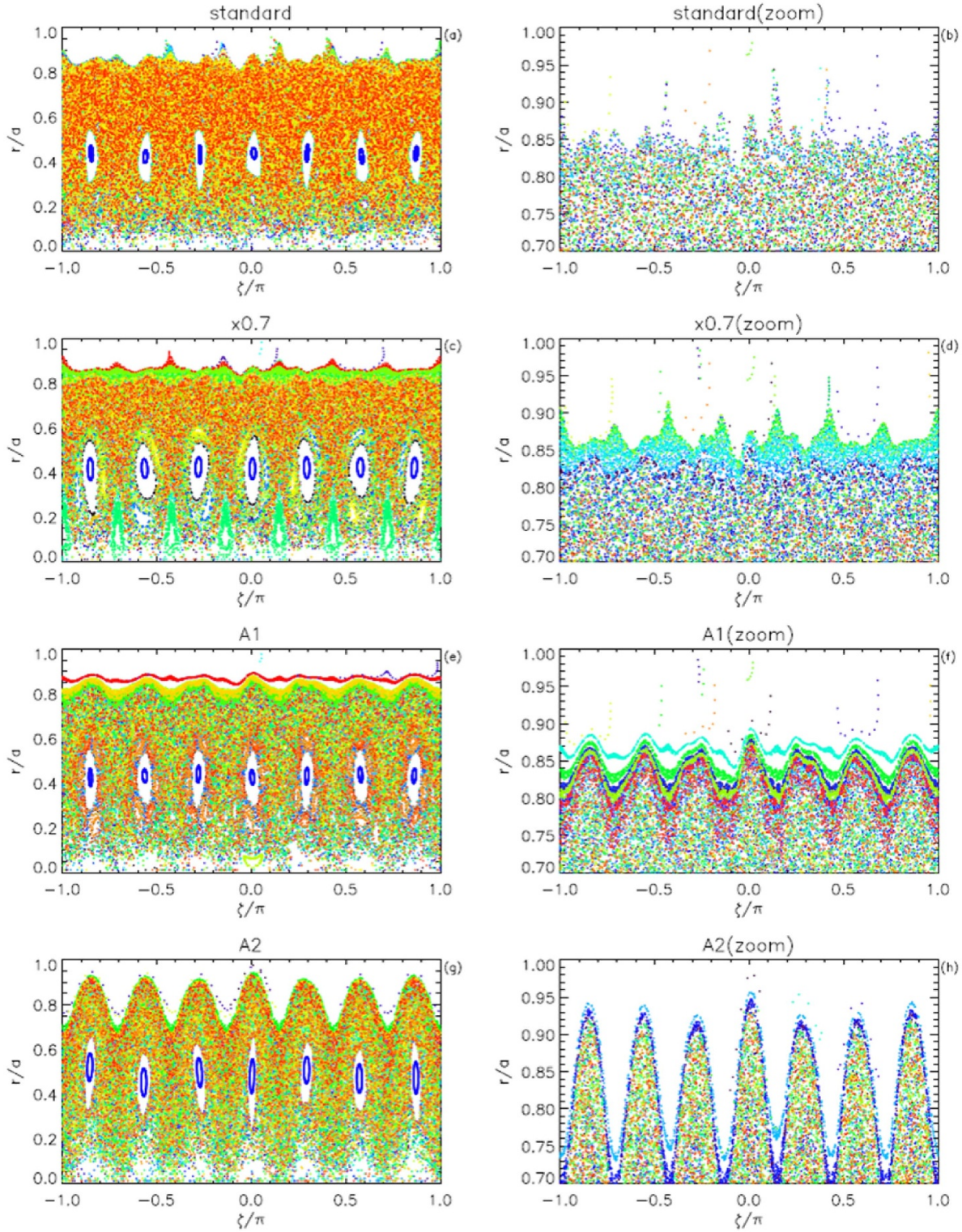

Figure 4. Poincaré maps from ORBIT (ζ is the Boozer toroidal angle and r the radial coordinate): left full radius, right zoom of plasma edge. (*a*), (*b*) Reference scenario; (*c*), (*d*) scaling of magnetic fluctuations by a factor 0.7; (*e*), (*f*) scaling of magnetic fluctuation according to spectrum A1; (*g*), (*h*) scaling of magnetic fluctuation according to spectrum A2.

respectively. Conserved magnetic surfaces with the periodicity of the dominant mode ($m = 1, n = 7$) appear close to the core surrounded by a partial chaotic field. In these plots the reconstruction of the field map has been performed considering the eigenfunctions of a reference past discharge at $I_p = 1.5$ MA during a QSH phase. No scaling of the mode amplitude has been performed, the equilibrium and the perturbations have only been adapted to the RFX-mod2 minor radius.

To evaluate the transport properties in this magnetic topology, ORBIT runs have been executed by using monoenergetic

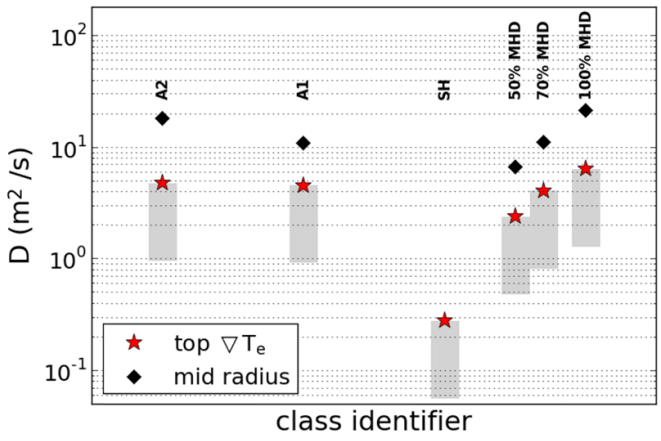

Figure 5. Particle diffusion coefficient (D) from ORBIT simulations considering different scaling of MHD perturbations. Shaded regions represent the range of values for the diffusion coefficient in the core region inside the transport barrier.

test particles subject to energy-conserving classical and pitch-angle collisions with a plasma background at the same temperature (assuming $T_i = 0.7 \times T_e$). Test electrons and ions are deposited in the region of interest with uniform pitch and their motion is integrated unless they reach a prescribed loss helical surface; they are then injected back in the helical axis position, in such a way to keep constant the particles number during the whole simulation, which lasts until a spatial stationary distribution of particles is reached. As described in [28, 29] from the outgoing flux of particles and from the gradient of their final distribution is easy to evaluate the corresponding local diffusion coefficient D. As reported in [30], an estimate of the ambipolar diffusion coefficient is obtained by the geometric average of the ion and electrons ones. The procedure just described has been applied to two regions: one near the top of the electron temperature gradient (edge of the helical core) and one at mid-radius (the chaotic region).

Following what was done in the analysis with ASTRA, the different estimates (for central and mid-radius) were computed also scaling the whole spectrum of secondary modes by a factor 0.7 and 0.5 while keeping constant the amplitude of the dominant mode (magnetic chaos is still present). The Poincaré maps corresponding to the 0.7 scaling are shown in figures 4(c) and (d), note that the reduced stochasticity allows other small conserved structures to appear around the one relative to the dominant mode. These structures are generated through non-linear secondary interaction between the modes included in the ORBIT simulation and though small they can affect transport.

The diffusion coefficients obtained by ORBIT are reported in figure 5 where stars represent the estimate at the top of the transport barrier while diamonds represent an estimate at mid-radius where a chaotic region is still present. The results show a trend similar to ASTRA with a significant reduction of particle transport expected in RFX-mod2, thanks to the reduced level of magnetic fluctuations. As a reference in the plot, we show also the ideal case of a pure single helicity state where neoclassical effects dominate in the transport mechanisms (no mid-radius estimate is shown for this case since no chaotic region is present given that flux surfaces are preserved). The grey shaded regions in figure 5 represent the range of values computed for the diffusion coefficient in the core region inside the internal transport barrier (i.e. the top of electron temperature gradient): transport reduces as particles move further into the core of the plasma from the transport barrier.

In the case of ORBIT analysis, as an additional test, instead of scaling each mode by a constant factor we also considered two spectra as estimated from stability evaluations (and corresponding growth rates for the TMs) expected for RFX-mod2 considering two extreme hypotheses for the current density profile, given the change in the shell proximity. We refer to the first spectrum as A1 (broad current density profile, similar to RFX-mod) obtained with a shape factor $e^{(7-n)/12}$ for $m = 1$ modes and a constant scaling factor 0.5 for $m = 0$ modes, and spectrum A2 (peaked current density profile) obtained with a shape factor $e^{(13-n)/6}$ for $m = 1$ modes and a constant scaling factor 0.35 for $m = 0$ modes. Poincaré maps corresponding to these scenarios are reported in figures 4(e)–(f) and (g)–(h) respectively. It is worth to note that while the edge region is clearly modified by the scaling of secondary modes, the changes in the core topology are less evident and more difficult to be appreciated without performing transport simulations.

As reported in figure 5, indeed, in these examples we see an improvement in particle confinement affecting mostly the edge (diamonds in figure 5) but overall also the core (see shaded regions figure 5). The effect is more pronounced for spectrum A1 where the amplitude of all the modes decreases with respect to RFX-mod. On the other hand for spectrum A2 the innermost modes actually increase and only secondary modes are reduced. This result can be taken as a qualitative indication of a possible range of variations for RFX-mod2, since the scaling factor (be it equal for the whole spectrum or different for each mode) is applied to the whole radial profile of each eigenfunction and this might not be correct for the new machine with the shell closer to the plasma.

Summarizing, both analyses (with ASTRA and ORBIT) do show a reduction in the expected particle transport for RFX-mod2 though using different approaches and internal assumptions: ASTRA is more sensitive to kinetic profiles (i.e. gradients), while ORBIT is probing confinement properties of the magnetic field structure.

As stated above, at the plasma edge a transport mechanism different from magnetic chaos is at play and it is likely to be ruled by coherent pressure structures (blobs) [31]. Consistently, both modelling and observation of magnetic data show that local topology is modified by the existence of a $q = 0$ resonance (in the RFP the safety factor q changes sign at plasma edge) and the corresponding toroidal chain of $m = 0$ islands, both in multiple helicity [32] and in helical [33] states. Also in the plasma external region (about 10% of the minor radius) stochastic transport is suppressed thanks to the local reduction of the $m = 1$ TM amplitude. This strongly affects PWI leading to a favourable extrapolation for RFX-mod2. In fact in the original RFX machine [34] (then modified and renamed RFX-mod [35]) PWI was dominated by the locking in phase of the $m = 1$ TMs (locked mode, LM) and 50% (about

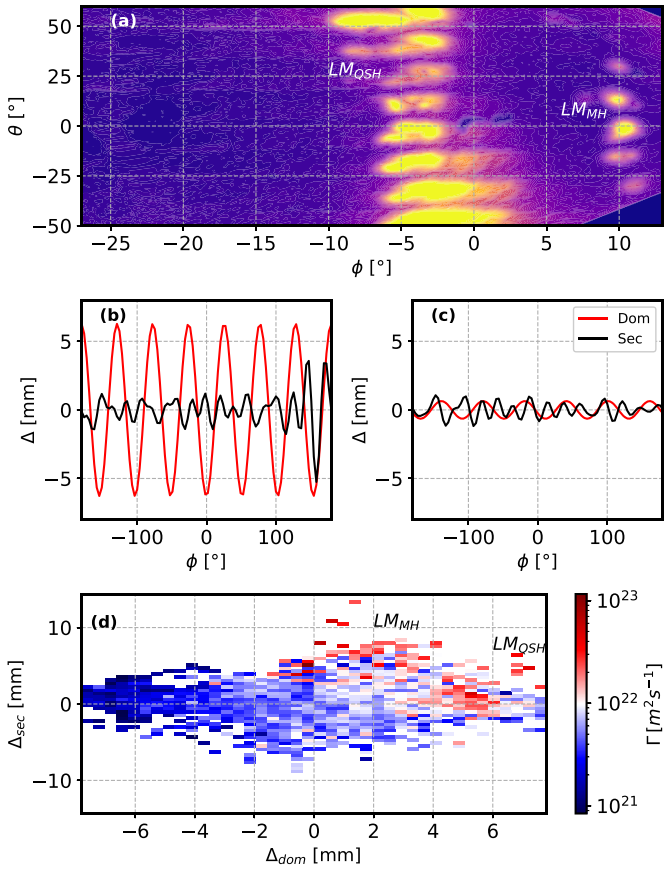

Figure 6. Camera image of the first wall for a pulse of RFX-mod (*a*). Local plasma deformation (Δ) associated to the dominant helicity (red) and secondary modes (black) for RFX-mod (*b*) and RFX-mod2 (*c*). Particle influxes as a function of the local plasma deformation due to dominant (Δ_{dom}) and secondary (Δ_{sec}) magnetic field modes (*d*).

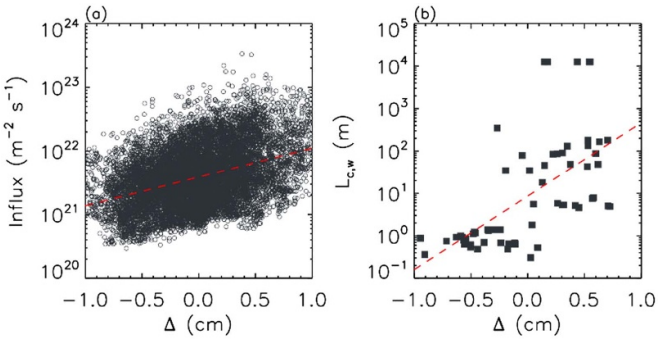

Figure 7. (*a*) Influxes as a function of total plasma deformation Δ; (*b*) scaling of the connection length (computed with the ORBIT code) as a function of total plasma deformation Δ. Red dashed lines provide an indication of an exponential trend.

80–100 MW m^{-3}) of the radiated power was lost at the LM [36]. In the RFX-mod machine [35], where a better control of MPs was available, PWI was not anymore dominated by the $m = 1$ LM which in this case was only responsible for about 18% of the total radiated power (with maximum values of 10 MW m^{-3}) [37]. Simulations of connection length with ORBIT highlight the role of ($m = 0$, $n = 7$) islands (produced by the dominant $m = 1$ helicity through toroidal coupling [33]) which become comparable to the LM with power spread over a larger surface [38, 39]. In figure 6(*a*) we show a camera image of the RFX-mod first wall that can be correlated with the map of the connection length from ORBIT highlighting the combined effect of $m = 0$ and $m = 1$ modes in defining the two hot spots (regions marked respectively LM_{QSH} and LM_{MH} in figure 6(*a*)). These results and ORBIT modelling [37] suggest a further decrease of PWI for RFX-mod2: the LM should disappear altogether and PWI should be dominated by $m = 0$ islands associated with the dominant helicity (figures 6(*b*) and (*c*)) with an estimated increase of the connection length by a factor 8.

In this respect, the correlation between the level of influxes and local plasma deformation (i.e. PWI) is shown in figure 6(*d*) where we present the effect of the two contributions mentioned above (locked mode and dominant mode): in either case (QSH plasmas marked LM_{QSH} and MH locked mode plasmas marked LM_{MH}) the reduction of the level of fluctuations leads to reduced particle influxes with the beneficial effects shown with ASTRA modelling in figures 2 and 3.

As a general remark (see figure 7(*a*)), a trend of the influxes (Γ) as a function of the total plasma deformation (Δ in cm) can be described with the scaling $\Gamma = \Gamma_0 \times \exp(\Delta/0.95)$ with $\Gamma_0 = 10^{21.6}$ m^2 s^{-1}, i.e. a reduction of the influxes by an order of magnitude every 2 cm of total shift reduction. This value (one order of magnitude) is the influx reduction which is expected in RFX-mod2.

The reduction can be estimated also in an independent way, by using the ORBIT code. We calculate the connection length to the wall by averaging the parallel length travelled along a bundle of 1000 field lines, all initiated at the same point on the equatorial plane. The simulation settings are those of RFX-mod, and they are the same as those used to produce figures 12(*a*) and (*b*) in [37]. In that paper, it was shown that the connection length $L_{c,w}$ follows a clear $n = 7$ pattern, with a minimum in the region of the phase locking of the secondary modes. Since the ideal displacement Δ shows the same $n = 7$ pattern superposed to the displacement of the locked mode, it is natural to plot the connection length as a function of Δ.

This is shown in figure 7(b): the connection length follows a trend that we can represent with an exponential dependence as a function of Δ, namely $L_{c,w} = L_0 \times \exp(\Delta/\Delta_0)$, with $L_0 \approx 8.6$ m and $\Delta_0 = 0.25$ cm. It is worth noting that connection length and influxes (figure 7(a)) follow a similar exponential dependence, though with a different characteristic (sheath) length Δ_0 (0.95 cm). This is not surprising, since the connection length is directly linked to the (outward) particle flux through $\Gamma = n_i \times \Delta \times v_{th}/L_{c,w}$ with n_i the ion density and v_{th} the thermal velocity, and the influx is in turn proportional to the outward flux of particles hitting the wall.

In this way, the change in connection length expected in RFX-mod2 can be taken as a proxy of the change in influxes: in [37] it was already estimated a change of a factor ≈8 in $L_{c,w}$, which is also the expected change in influx calculated with ORBIT. This number is consistent with the result mentioned

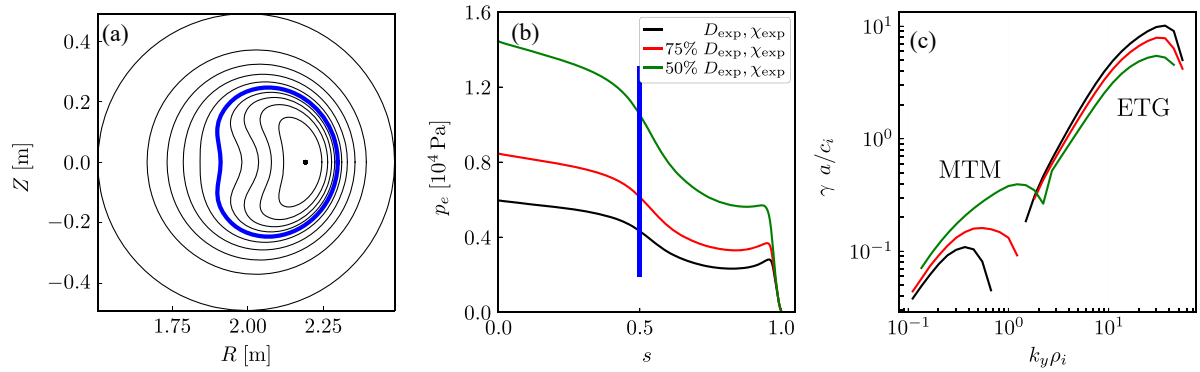

Figure 8. (*a*) Flux surfaces section ($\phi = 0$) for the VMEC equilibrium of figure 2, with the surface $s = \psi_t/\psi_{t,edge} = 0.5$ (in blue) corresponding to the mid electron temperature barrier. (*b*) Pressure profiles for the three cases obtained with the rescaled transport coefficients. (*c*) Corresponding linear GENE calculations of the growth rate γ as a function of the wavenumber $k_y\rho_i$ at $s = 0.5$.

above estimated from the fit of the influxes as a function of the total plasma deformation based on RFX-mod data.

For the three cases shown in figure 2, resulting from ASTRA simulations with nominal and rescaled transport coefficients, we have investigated the occurrence of micro-instabilities in the region of the electron temperature barrier with the gyrokinetic code GENE [40]. For this purpose we have first extended the RFX-mod wall to $a = 0.491$ m and built the corresponding VMEC [41] equilibria with $(m,\ n) = (1,7)$ helicity, simply increasing the plasma volume and toroidal flux, and assuming the same q profile. A force-free approximation is assumed, thus forcing the same magnetic equilibrium for the three cases with different pressure, see figures 8(*a*)–(*c*). In the figure, the surface $s = \psi_t/\psi_{t,edge} = 0.5$ (highlighted in blue) is the radial position where the logarithmic gradient of the electron temperature $1/L_{Te} = -{T_e}^{-1}/\mathrm{d}T_e/\mathrm{d}s^{1/2}$ reaches its maximum, $1/L_{Te} \sim 4$, very similar for the three cases and only slightly decreasing for the profiles with reduced D and χ coefficients—from 100% to 50%. On the other hand, even if the density profiles remain rather flat, their logarithmic gradient increases when D and χ are lowered, reaching the value $1/L_{ne} \sim 0.1$ for the case '50% D_{exp}, χ_{exp}'. As a result, the ratio $\eta_e = L_{ne}/L_{Te}$ decreases for reduced global transport coefficients. At the same time, the pressure increases everywhere, bringing to higher local values of β. As is known, the two parameters η_e and β have important implications on electrostatic and electromagnetic instabilities and turbulence.

Following the procedure described in [42], we have applied the geometric interface code GIST [43] to one of the two stellarator-symmetric flux tubes, in particular the tube originating from the outboard midplane at $\phi = 0$. On the basis of the study carried out in [42], this choice does not modify our conclusions, as similar growth rates and turbulence levels are expected to take place for the two opposite flux tubes, see [44] for further details on this argument.

For the case with the nominal values of the transport coefficients D_{exp} and χ_{exp}, the most unstable modes are microtearing modes (MTMs) for $k_y\rho_i < 1$ and electron-temperature-gradient (ETG) modes for $k_y\rho_i > 1$, which appear as distinct branches in the linear spectrum. This is in agreement with the results reported in [42], where these two instabilities are found to characterize several helical states in the RFX-mod database. For the cases with decreased global coefficients D and χ, the MTM growth rates and wavenumbers increase significantly due to large local increase of the plasma β, while the ETG growth rates decrease, due to the reduction of η_e. The two branches now overlap in a large part of the linear spectrum.

The reduction of the global D and χ coefficients thus provides scenarios with higher and more peaked density profiles, which imply larger MTM and lower ETG growth rates. These two instabilities mainly impact the electron heat transport, the former being electromagnetic in nature and causing heat transport at ρ_i-scales through small scale magnetic stochasticity, the latter being electrostatic, mainly active at ρ_e-scales. The interaction between MTM and ETG turbulence is a multiscale problem, addressed in previous works only in axisymmetric geometry, which is expected to cause MTM turbulence to be suppressed by ETG modes due to the breaking of current sheets by small-scale $E \times B$ flows [45], and a simultaneous suppression of the ρ_e-scale heat fluxes by large/intermediate-scale zonal flows induced by MTM turbulence [46]. The consequent reduction of the total electron heat flux via cross-scale interaction is further discussed in [47]. In our case, the mutual interaction between MTM and ETG turbulence is expected to be enhanced at higher and peaked density, in the cases with low D and χ coefficients. However, the possible reduction of the total electron heat flux should be verified and quantified through computationally expensive multiscale simulations, also including the 3D geometry of the equilibria.

3. Plasma control and stability

RFX-mod performed state-of-the-art mode control experiments thanks to its flexible MHD control system [48]. In the RFX-mod2 device, the control of MHD modes (TMs and resistive wall modes (RWMs)) on the one hand will be facilitated by the smaller plasma-shell distance but on the other hand the new front-end structure could result in a destabilizing effect. The upgraded MHD plasma control system will be crucial to the experiments and the ongoing predictive analyses

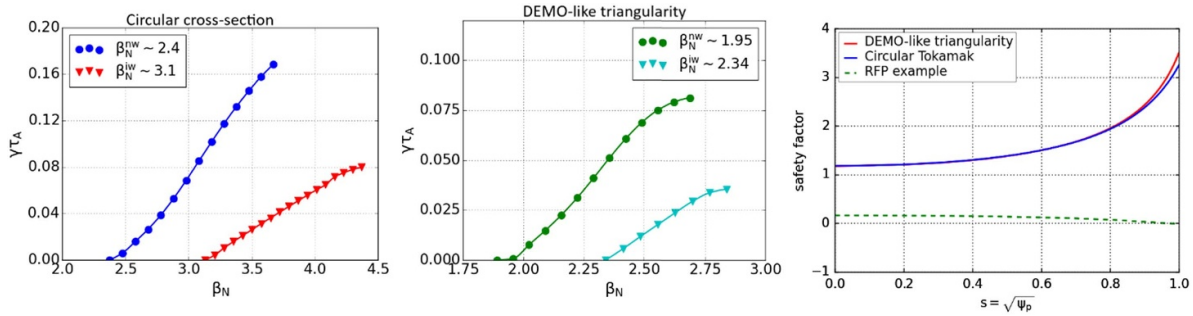

Figure 9. Stability scan of the ideal kink without a wall (blue and green) and with an ideal wall (red and cyan) for a circular tokamak and a DEMO-like D-shaped tokamak. We show q profiles for both cases and for comparison also a typical RFP q profile (the radial coordinate is the square root of the poloidal flux).

will provide important information to prepare the experimental programme.

The control system is undergoing a new design as magnetic diagnostics on RFX-mod2 have been largely extended [49] in both spatial and time resolution: the saddle loops and pick-up coils for MHD mode activity detection and feedback control, are now 8 × 72 (from 4 × 48, poloidal by toroidal direction), with a bandwidth increased to 200 kHz from the previous 2 kHz.

A modelling framework has been implemented, including the updated saddle coil geometry and new tri-axial pick-up probes, based on the MARS-F linear resistive MHD code [50]. This code is also used to assess the preliminary stability boundaries foreseen in RFX-mod2 Tokamak plasmas [51], while an investigation of ideal and resistive stability in RFP configurations is presently ongoing. The analysis scheme requires as a first step the representation of equilibria with the CHEASE equilibrium code [52] that was revamped in order to model also RFP equilibria and takes advantage of the EQDSK representation of equilibria computed for RFX-mod from experimental data and for RFX-mod2 as synthetic cases.

For the latter case the ($m = 1$, $n = 6$) RWM was analysed estimating its growth rate as a function of shell proximity. The additional goal is to provide a comparison between RFX-mod and RFX-mod2 in order to understand if a higher level of flexibility can be reached in the new machine in terms of plasma shaping and control. As observed in transport modelling, the new machine is expected to improve also in terms of RWM control. Starting from a no-wall condition the growth rate $\gamma_{(m,n)}$ of some external kink modes is significant: $(\gamma\tau_A)_{1,6} = 0.68$, $(\gamma\tau_A)_{1,5} = 0.91$, $(\gamma\tau_A)_{1,4} = 0.98$ (τ_A is the Alfvén time). Adding the resistive wall (we focus on the $n = 6$ mode) drastically reduces the growth rates down to the RWM regime ($\gamma\tau_W \sim 1$): for RFX-mod $(\gamma\tau_A)_{1,6} = 2.6 \times 10^{-4}$ (as experimentally observed). A further reduction to $(\gamma\tau_A)_{1,6} = 1.7 \times 10^{-4}$ is expected for RFX-mod2.

In the tokamak configuration, given the flexibility of RFX-mod2 in shaping tokamak plasmas and being the optimization of plasma shape in terms of its stability one of the major goals of the future experimental campaign, we investigated the stability of the $n = 1$ ideal kink as well as $n = 1$ TMs for two tokamak scenarios: a circular cross section plasma and a DEMO-like D-shaped plasma [53]. We note that in this study plasma current is assumed constant along the pressure scan, allowing global conservation of the safety factor as well (within acceptable limits). The q profile for the two configurations is shown in figure 9 compared to a typical profile for the RFP.

As for the ideal kink, (figure 9) we see that considering a target $\beta_N \sim 0.75$ the configuration is safely stable to pressure driven external kink ideal modes (we can still encounter the internal kink associated to sawtoothing activity). It is to note that compared to the circular cross-section, the shaped equilibrium has lower no-wall as well as ideal-wall stability limits, and a considerably narrower wall-stabilized region.

For both plasmas (circular and D-shaped) we find that TMs are unstable and in particular for the analysed equilibria we find a dominant eigenfunction at the $q = 2$ resonance surface. In terms of the scaling of the growth rate we find the expected trend as a function of the Lundquist number ($\sim S^{-3/5}$) so that these modes may appear in RFX-mod2 plasmas depending on the S regime that will be explored (in RFX-mod we operated around a value of 10^4) and possibly may lead to NTM as well.

As in RFX-mod also in the new machine the main goal will be to address control strategies in different scenarios and configurations. In this respect for the purpose of RWM control assessment, an updated 'flight-simulator' is being developed. This tool has been successfully benchmarked in the past against RWM growth rates from RFX-mod experiments [54] and a similar concept has been developed for JT-60SA [55]. Active control of RWMs is in fact a common issue to RFP and high β Tokamak operation. Although different physics are usually at play, with the Ohmic RFP lacking much of the rotation-triggered effects which are thought to influence stability in Tokamaks, magnetic control can be addressed in the same way when necessary.

To this end the coupling between MARS-F and Cariddi [56]. The former code is used to compute linear ideal plasma response to generic external fields while the latter solves the 3D eddy current problem with realistic geometry of passive and active structures. In particular, a mesh was developed to describe the RFX-mod2 shell including both poloidal and toroidal gaps (though presently in a simplified way, i.e. not

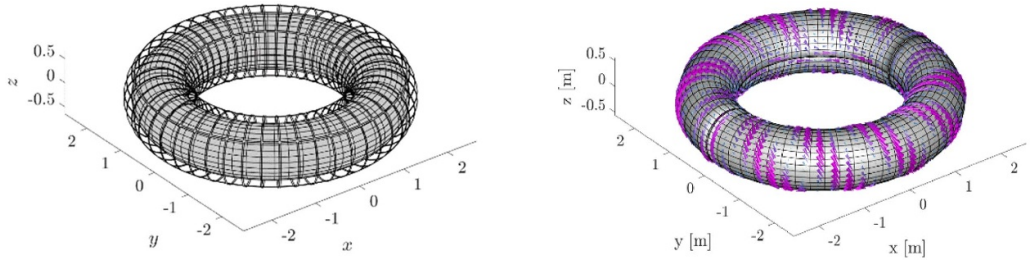

Figure 10. Left: mesh for the 3D shell with equatorial gaps and two poloidal gaps, and saddle coils. Right: $n = 6$ eigenvector on 3D shell with gaps.

modelling the overlapped poloidal gap) and the new magnetic sensors layout (figure 10 left). The coupling of these two codes is done with the CarMa approach described in [57] thus taking into account the real geometry of conducting structures. We will refer to this as CarMa model in the following.

In figure 10 (right) we show the eigenvalue of wall currents due to an $n = 6$ mode on the realistic 3D wall. This is part of the consistency checks between MARS-F and CarMa which are now focussing on RWM growth rates estimates, before going to the full integration of the two codes and the development of the full control scheme loop with the realistic 3D wall.

Nevertheless, feedback control of the $m = 1$, $n = 6$ RWM has been investigated with the MARS-F code, which allows external currents (i.e. coils) to be included in the modelling domain. Differently from the CarMa model, for direct feedback a simplified geometry of RFX-mod2 active coils is implemented in terms of radial distance from the plasma and poloidal length of the coil legs. Feedback control has been applied with a proportional scheme, using both poloidal and radial measurements as feedback variables. These virtual measurements are taken at the radius of the saddles sensors that will be installed on RFX-mod2. Figure 11 reports the results of these first simulations varying the proportional gain K_p, suggesting that poloidal field sensors could be more effective. On one hand this is consistent with most of the RWM active control results in tokamaks, on the other it should be reminded that control schemes based on tailored processing of the radial field measurements were successfully applied in RFX-mod. In fact, the control of RWM in RFP discharges was performed by using the raw harmonic components of the radial field. Conversely, the control of TMs in RFP discharges and $m = 2$, $n = 1$ RWM in tokamak discharges required the removal of the sidebands due to the active coils action from the corresponding feedback harmonic component. Analyses based on theoretical models showed the effect of sensors and coils number and periodicity on the active control of MHD modes [58]. The main message we can get from figure 11 is that an $n = 6$ RWM can be stabilized, with results to be compared with the CarMa model being developed.

Once the 'flight simulator' is thoroughly checked the tool will be used to investigate the effect of the close-fitting copper shell, compared to RFX-mod, in the main plasma scenarios that the new device is designed to explore. In particular for the RFP case, we will address the stabilization of multiple RWMs

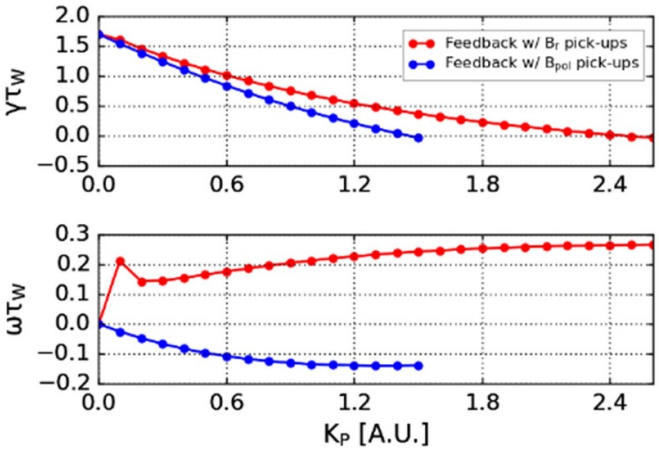

Figure 11. Testing proportional control (K_p is the proportional gain) of $n = 6$ mode with either poloidal (blue) or radial (red) point-like field as feedback variable.

with different sensor geometries, comparing their effectiveness in terms of coil current requirements.

4. Shaped tokamak scenario

RFX-mod2 will continue tokamak studies started in RFX-mod focusing on shaped plasmas with both positive and negative triangularity, given the results in terms of stability and performances observed on different machines in the latter configuration [59].

In this respect the effect of the close-fitting copper shell is being investigated in the shaped tokamak case where the non-uniform plasma–wall distance can significantly affect mode stability. This can be even more critical and require proper plasma shape definition in negative triangularity scenarios as well as in snowflake configuration, particularly with low safety factor in the plasma edge. Preliminary studies have been addressed in [51] and [60], which need to be validated and expanded in terms of experimental operation and modelling that will be dedicated to these scenarios.

The analysis shown in the previous section for a D-shaped plasma, has been extended to single-null configurations both with positive and negative triangularity (see figure 12 left for the latter shape). A linear analysis shows that both plasma

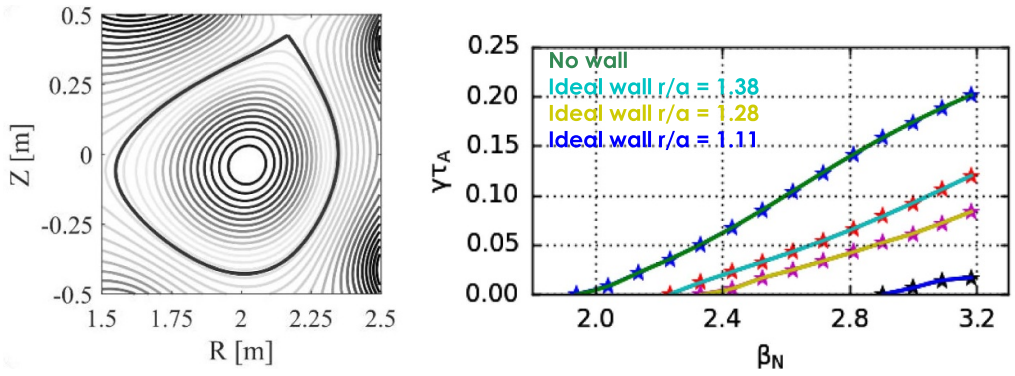

Figure 12. Left: negative triangularity plasma with $q(a) > 2$ (the thick line represents the separatrix). Right: ($m = 2$, $n = 1$) growth rate for different shell proximity values. Extrapolation to $b/a = 1.04$ results in a safe regime.

shapes are stable to ideal MHD low-n modes (excluding the (1,1) internal kink) in the L-mode scenario. More physics is going to be included in the model, starting from resistivity, to grasp the effects of shaping and triangularity on the stability of TMs.

As for the DEMO-like case, we investigated the trend with β_N of the growth rate of the (2,1) pressure driven mode for the negative triangularity plasma with different values of plasma-shell proximity. As shown in figure 12 right we do expect a favourable condition in the regimes that we can produce in RFX-mod2 where $b/a = 1.04$.

Another important issue related to the optimization of the plasma configuration is the vertical stability. Comparing the positive and negative triangularity cases, the latter one appears to be more unstable with respect to the former. As the negative triangularity configuration was obtained mirroring the positive one, this procedure has an effect in terms of local geometrical features such as a larger distance from the plasma to the passive stabilizing shell in the low-field side. This aspect will be part of the optimization in view of the experimental campaigns.

From the point of view of microturbulence, given the shape of kinetic profiles (density and temperature) observed in RFX-mod, the focus was on instabilities driven by temperature gradients. To this end in the simulations for these tokamak shaped plasmas [51], the density profile was represented as flat for a large part of the volume with a gradient only at the edge. Within these assumptions, the analysis shows the advantages moving from positive to negative triangularity in terms of energy confinement in TEM-dominated or mixed ITG/TEM turbulent regimes. The modelling shows that at mid radius the most unstable modes are ITG while ETG modes become more important at the edge where density gradient develops. As far as TEM modes are concerned, lower fluctuation levels in both density and temperature are obtained in negative triangularity plasmas.

We remark that the results obtained (apart from basic assumptions due to the unknown plasma features of the new machine) strongly depend on how some quantities like the local magnetic shear and curvature interact with the mode structure. From this point of view the plasma shaping capability of RFX-mod2 offers the possibility to fine-tune the plasma geometry to reduce the energy transport in the electron channel, ion channel or both.

5. Conclusion

RFX-mod2 is scheduled to start operation in 2025 and will cover both RFP and tokamak plasma configurations. In this work we presented first predictive scenario studies in terms of transport, stability and turbulence properties of both RFP and tokamak (circular and shaped) plasmas as well as the upgrade of control modelling codes. These analyses will continue with the goal of optimizing plasma configuration, shaping and control schemes, in order to prepare the initial experimental campaign and the tools useful for control room analysis and data sharing during experiments.

The advanced RFX-mod2 diagnostics in preparation to measure internal kinetic profiles will allow a better experimental characterization and provide additional input to the codes in terms of time evolution of temperature profiles, particle sources (both main gas and impurities) and neutrons production. Based on the upgraded diagnostics capabilities of RFX-mod2, high frequency magnetic and electrostatic fluctuation measurements will be possible in the scrape off layer and plasma edge, allowing for a remarkably detailed characterization of turbulence in that region. The operation of RFX-mod2 will also allow the optimization of a new controller based on the new reflectometric diagnostic to control both vertical and horizontal position of plasma equilibrium (circular and shaped).

An important research line will be the exploitation of the RFX-mod2 active control system for ELM mitigation studies. This is motivated by the experience on RFX-mod operations, where ohmic and edge biasing induced transitions to H-mode (by means of a polarized electrode) could be reproducibly achieved also in shaped discharges, with important modifications of the edge plasma density and flow properties [61].

ORCID iDs

D. Terranova https://orcid.org/0000-0001-9339-283X
M. Agostini https://orcid.org/0000-0002-3823-1002
F. Auriemma https://orcid.org/0000-0002-1043-1563
M. Gobbin https://orcid.org/0000-0001-5261-3683
G. Marchiori https://orcid.org/0000-0001-9369-5486
L. Pigatto https://orcid.org/0000-0002-0556-0440
P. Porcu https://orcid.org/0000-0002-5040-4885
I. Predebon https://orcid.org/0000-0002-2100-4698
G. Spizzo https://orcid.org/0000-0001-8586-2168
N. Vianello https://orcid.org/0000-0003-4401-5346
P. Zanca https://orcid.org/0000-0003-3208-976X
D. Abate https://orcid.org/0000-0002-0331-3454
D. Bonfiglio https://orcid.org/0000-0003-2638-317X
M. Bonotto https://orcid.org/0000-0001-9147-7506
S. Cappello https://orcid.org/0000-0002-2022-1113
R. Lorenzini https://orcid.org/0000-0001-8353-4857
L. Marrelli https://orcid.org/0000-0001-5370-080X
M. Veranda https://orcid.org/0000-0002-5821-2896
M. Zuin https://orcid.org/0000-0002-0282-2978

References

[1] Marrelli L. *et al* 2019 *Nucl. Fusion* **59** 076027
[2] Peruzzo S. *et al* 2023 *Fusion Eng. Des.* **194** 113890
[3] Zuin M. *et al* 2022 *Nucl. Fusion* **62** 066029
[4] Bonfiglio D., Cappello S., Piovan R., Zanotto L. and Zuin M. 2008 *Nucl. Fusion* **48** 115010
[5] Carraro L. *et al* 2023 *29th Fusion Energy Conf. (IAEA-FEC)* (*London, UK*, *16–21 October*) p EX–C/2061
[6] Terranova D. *et al* 2010 *Plasma Phys. Control. Fusion* **52** 124023
[7] Marrelli L. *et al* 2021 *Nucl. Fusion* **61** 023001
[8] Gobbin M., Franz P., Auriemma F., Lorenzini R. and Marrelli L. 2015 *Plasma Phys. Control. Fusion* **57** 095004
[9] Bonfiglio D. *et al* 2019 *46th EPS Conf.* (*Milan, Italy*, *8–12 July 2019*) (available at: http://ocs.ciemat.es/EPS2019PAP/pdf/P1.1049.pdf) p P1.1049
[10] Spinicci L. *et al* 2022 *48th EPS Conf.* (*Maastricht, The Nederlands*, *27 June–1 July 2022*) (available at: https://indico.fusenet.eu/event/28/contributions/23/) p P5b.102
[11] Veranda M. *et al* 2017 *Nucl. Fusion* **57** 116029
[12] Marrelli L. *et al* 2021 *28th Fusion Energy Conf. (IAEA-FEC), Virtual Conf.* (*10–15 May*) p EX/P7–4 (available at: www.iaea.org/events/fec-2020)
[13] Yambe K., Hirano Y., Sakakita H. and Koguchi H. 2014 *Phys. Plasmas* **21** 114502
[14] Sarff J.S. *et al* 2015 *Nucl. Fusion* **55** 104006
[15] Auriemma F. *et al* 2015 *Nucl. Fusion* **55** 043010
[16] Gobbin M. *et al* 2022 *Nucl. Fusion* **62** 026030
[17] Momo B. *et al* 2020 *Nucl. Fusion* **60** 056023
[18] Lorenzini R., Terranova D., Alfier A., Innocente P., Martines E., Pasqualotto R. and Zanca P. 2008 *Phys. Rev. Lett.* **101** 025005
[19] Carraro L. *et al* 2013 *Nucl. Fusion* **53** 073048
[20] Pereverzev G.V. *et al* 2002 IPP technical report 02 (Max-Planck Institut fur Plasmaphysik)
[21] White R.B. and Chance M.S. 1984 *Phys. Fluids* **27** 2455
[22] Rechester A.B. and Rosenbluth M.N. 1978 *Phys. Rev. Lett.* **40** 38
[23] Spolaore M., Antoni V., Spada E., Bergsåker H., Cavazzana R., Drake J.R., Martines E., Regnoli G., Serianni G. and Vianello N. 2004 *Phys. Rev. Lett.* **93** 215003
[24] Vianello N., Spolaore M., Serianni G., Bergs ker H., Antoni V. and Drake J.R. 2002 *Plasma Phys. Control. Fusion* **44** 2513
[25] Serianni G., Murari A., Fiksel G., Antoni V., Bagatin M., Desideri D., Martines E. and Tramontin L. 2001 *Plasma Phys. Control. Fusion* **43** 919–27
[26] Agostini M. and Scarin P. 2020 *Plasma Phys. Control. Fusion* **62** 025009
[27] Giacomin M. and Ricci P. 2020 *J. Plasma Phys.* **86** 905860502
[28] Spizzo G., White R.B. and Cappello S. 2007 *Phys. Plasmas* **14** 102310
[29] Gobbin M., Marrelli L., Martin P. and White R.B. 2007 *Phys. Plasmas* **14** 072305
[30] Predebon I., Marrelli L., White R.B. and Martin P. 2004 *Phys. Rev. Lett.* **93** 145001
[31] Agostini M., Scarin P., Spizzo G., Vianello N. and Carraro L. 2014 *Plasma Phys. Control. Fusion* **56** 095016
[32] Spizzo G., Cappello S., Cravotta A., Escande D.F., Predebon I., Marrelli L., Martin P. and White R.B. 2006 *Phys. Rev. Lett.* **96** 025001
[33] Martines E., Lorenzini R., Momo B., Munaretto S., Innocente P. and Spolaore M. 2010 *Nucl. Fusion* **50** 035014
[34] Rostagni G. 1995 *Fusion Eng. Des.* **25** 301
[35] Sonato P. *et al* 2003 *Fusion Eng. Des.* **66–68** 161
[36] Marrelli L., Zanca P., Martin P., Martini S. and Murari A. 1999 *J. Nucl. Mater.* **266–9** 877
[37] Scarin P., Agostini M., Spizzo G., Veranda M. and Zanca P. 2019 *Nucl. Fusion* **59** 086008
[38] Porcu P., 2022 3D plasma-wall interaction in the RFX-mod device *Master's thesis* Università di Padova
[39] Spizzo G. *et al* 2023 *16th Chaotic Modeling and Simulation Int. Conf.—CHAOS* (*Herakleion, Greece*, *13–17 June*) (available at: http://www.cmsim.org/chaos2023.html)
[40] JENKO F., Dorland W., Kotschenreuther M. and Rogers B.N. 2000 *Phys. Plasmas* **7** 1904
[41] Hirshman S.P. and Whitson J.C. 1983 *Phys. Fluids* **26** 3554
[42] Predebon I., Xanthopoulos P. and Gobbin M. 2019 *Plasma Phys. Control. Fusion* **61** 055011
[43] Xanthopoulos P., Cooper W.A., Jenko F., Turkin Y., Runov A. and Geiger J. 2009 *Phys. Plasmas* **16** 082303
[44] Predebon I. and Xanthopoulos P. 2015 *Phys. Plasmas* **22** 052308
[45] Maeyama S., Watanabe T.-H. and Ishizawa A. 2017 *Phys. Rev. Lett.* **119** 195002
[46] Pueschel M.J., Hatch D.R., Kotschenreuther M., Ishizawa A. and Merlo G. 2020 *Nucl. Fusion* **60** 124005
[47] Maeyama S., Watanabe T.-H., Nakata M., Nunami M., Asahi Y. and Ishizawa A. 2022 *Nat. Commun.* **13** 3166
[48] Ortolani S. (the RFX Team) 2006 *Plasma Phys. Control. Fusion* **48** B371
[49] Marconato N., Bettini P., Cavazzana R., Grando L., Marchiori G., Marrelli L., Peruzzo S. and Pomaro N. 2019 *Fusion Eng. Des.* **146** 906
[50] Liu Y.Q., Bondeson A., Fransson C.M., Lennartson B. and Breitholtz C. 2000 *Phys. Plasmas* **7** 3681
[51] Predebon I., Abate D. and Pigatto L. 2022 *Nucl. Fusion* **62** 066039
[52] Lütjens H., Bondeson A. and Sauter O. 1996 *Comput. Phys. Commun.* **97** 219
[53] Abate D., Marchiori G., Bettini P. and Villone F. 2020 *Plasma Phys. Control. Fusion* **62** 085001
[54] Marchiori G., Baruzzo M., Bolzonella T., Liu Y.Q., Soppelsa A. and Villone F. 2012 *Nucl. Fusion* **52** 023020

[55] Pigatto L. *et al* 2019 *Nucl. Fusion* **59** 106028
[56] Albanese R. and Rubinacci G. 1998 *Adv. Im. El. Phys.* **102** 1–86
[57] Albanese R., Liu Y.Q., Portone A., Rubinacci G. and Villone F. 2008 *IEEE Trans. Magn.* **44** 1654–7
[58] Zanca P., Marrelli L., Paccagnella R., Soppelsa A., Baruzzo M., Bolzonella T., Marchiori G., Martin P. and Piovesan P. 2012 *Plasma Phys. Control. Fusion* **54** 094004
[59] Marinoni A., Sauter O. and Coda S. 2021 *Rev. Mod. Plasma Phys.* **5** 6
[60] Abate D., Predebon I., Bonotto M. and Marchiori G. 2023 *Fusion Eng. Des.* **189** 113484
[61] Spolaore M. *et al* 2017 *Nucl. Fusion* **57** 116039